# Valence shell charge concentrations and the Dewar–Chatt–Duncanson bonding model†

**Wolfgang Scherer,*[a] Georg Eickerling,[a] Dmitry Shorokhov,[a] Emanuel Gullo,[b] G. Sean McGrady[c] and Peter Sirsch[c]**

*Received (in Durham, UK) 26th October 2005, Accepted 6th January 2006*
*First published as an Advance Article on the web 3rd February 2006*
**DOI: 10.1039/b515171f**



**Combined experimental and theoretical charge density studies of the complex [Ni($\eta^2$-$C_2H_4$)dbpe] (dbpe = $Bu^t_2PCH_2CH_2PBu^t_2$), 1, reveal how the location and magnitude of charge concentrations in the valence shell of the metal atom influence the σ- and π-components of the metal–olefin interaction.**

The Dewar–Chatt–Duncanson (DCD) model for $\eta^2$-coordination of an olefin ligand to a transition metal centre has proved to be one of the most elegant and versatile concepts in organometallic chemistry over the past half-century,[1] and its facile extension to encompass also σ-bond complexes[2] emphasises its general utility in analysing non-classical metal–ligand bonding. Earlier theoretical studies of the model nickel olefin complex [Ni($\eta^2$-$C_2H_4$)($PH_3$)$_2$] **1a** showed it to be an ideal benchmark system to analyse the σ- and π-components of the metal-olefin interaction, since the 14-electron fragment [Ni($PH_3$)$_2$] is neither particularily Lewis-acidic nor basic.[3] MO analyses of **1a** confirmed that σ donation and π back-donation are both present in **1a**, although the latter contribution is dominant.[3]

The dominant olefin ← Ni π back-donation in **1a** is almost exlusively accommodated by the HOMO-4 ($b_2$ symmetry; Fig. 1c), and leads to a charge transfer from the Ni $d_{yz}$ orbital into the antibonding π* orbital of the olefin ligand. The reverse olefin → Ni charge transfer, however, is more complex and involves a total of four orbitals (all $a_1$ symmetry), which represent donation from the C=C π bond and the C–C σ bond into $d_{x^2-y^2}$ and $d_{z^2}$ orbitals at the metal. A similar complex bonding situation was found by Frenking *et al.* for the heavier Group 10 model complex [Pt($\eta^2$-$C_2H_4$)($PH_3$)$_2$] **1b** by a charge decomposition analysis.[4] Hence, the simple DCD picture of the olefin → Ni donation, which assumes an interaction between the occupied π orbital of the olefin and a suitable d-orbital at the metal (as displayed by the HOMO-5 in Fig. 1a), may be an oversimplification for many transition metal–olefin complexes. In the light of these complications with the MO picture, analysis of the topology of the total charge density offers distinct advantages in dealing with these complex bonding features.

These advantages were recognised by Macchi *et al.* in a pioneering experimental charge density analysis of [Ni(COD)$_2$] **1c** which exploited Bader's powerful atoms in molecules (AIM) methodology.[5] According to the authors, both σ donation and π back-donation were identified in the Ni–C bond paths of **1c**, which are concave owing to charge accumulation inside the $NiC_2$ ring fragment by σ donation, but are also well separated as a result of the π back-donation.[6] However, a more complex bond path scenario emerges from our combined experimental and theoretical charge density analysis of our experimental system [Ni($\eta^2$-$C_2H_4$)dbpe] **1** (Fig. 2) which is coordinated by a chelating phosphine ligand and displays similar bonding features to the model system **1a**.[7] Fig. 3 shows the experimental and theoretical contour maps of the Laplacian of the charge density, $\nabla^2\rho(\boldsymbol{r}) = -L(\boldsymbol{r})$, in the $NiC_2$ plane of **1**, along with the superimposed bond paths. The experimental and theoretical bond paths in **1** display a more complex profile than the previous study of **1c**,[6] with two points of inflection: the Ni–C bond path curvature changes from endocyclic through exocyclic and back again to endocyclic. We note, that the curvature of the Ni–C bond path is generally less pronounced in the experimental study, and its complex nature is only revealed when a highly flexible multipolar model is used for the Ni and the C atoms. This arises from the flatness of the charge density distribution inside the $NiC_2$ metallacycle about the ring critical point (RCP). Accordingly, the charge density inside the ring and that at the M–C bond critical points (BCPs) does not differ significantly in **1**, a scenario characteristic also of the β-agostic protonation product of **1**, *viz.* $[C_2H_5Ni(dbpe)]^+$.[11] In the case of **1**, $\rho(\boldsymbol{r})$ at the RCP and at the Ni–C BCPs amounts to 0.65/[0.68] and 0.67/[0.72] $e$Å$^{-3}$, respectively (average values for the BCPs; theoretical values in brackets). The flatness of the charge density distribution around the RCP is also reflected in high bond ellipticities at the Ni–C BCPs (average values 1.04/[0.87]). Hence, small changes in the charge density in the NiCC bonding region have a significant influence on the bond path profile.

The major differences in the bond path topology of **1** between theory and experiment are found in the region around the Ni–C BCP, where the experimental bond path is nearly linear but the calculated one is clearly exocyclic. This might indicate an underestimation of charge transfer due to π back-donation by the multipolar model used in the experimental study. Fig. 1c shows the Kohn–Sham orbital (HOMO-4)

[a] *Institut für Physik, Universität Augsburg, Universitätsstr. 1, D-86135 Augsburg, Germany. E-mail: wolfgang.scherer@physik.uni-augsburg.de; Fax: +49-(0)821-598-3227; Tel: +49(0)821-598-3350*
[b] *Department of Chemistry, University of Bath, Claverton Down, Bath, UK BA2 7AY*
[c] *Department of Chemistry, University of New Brunswick, Fredericton, NB, Canada E3B 6E2*

† Electronic supplementary information (ESI) available: Crystallographic data and results of topological analysis of compound **1**. See DOI: 10.1039/b515171f

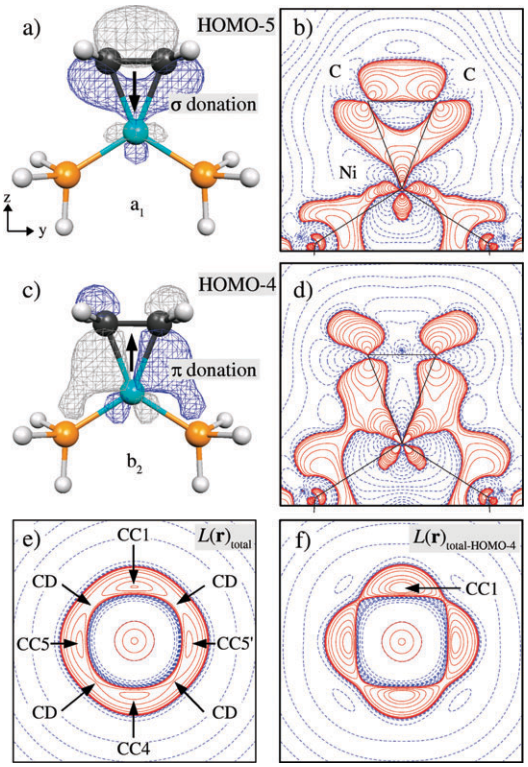


**Fig. 1** (a, c) Kohn–Sham orbitals of HOMO-5 and HOMO-4 of **1a**, respectively. (b, d) $L(\boldsymbol{r})$ contour maps of the charge density contribution in the NiC1C2 plane from HOMO-5 and HOMO-4, respectively. HOMO-5 is one of 4 orbitals of $a_1$ symmetry of **1a** which contribute to the olefin → Ni donation. (e) $L(\boldsymbol{r})$ contour maps of the total charge density and (f) after substracting the density contribution of HOMO-4. Default contour levels as defined in Fig. 3.

responsible for back-donation in our model system **1a**, and Fig. 1d its corresponding $L(\boldsymbol{r})$ contour map. The contribution of this MO to the total charge density will encourage exocylic curvature of the bond path as displayed in Fig. 3b. This contribution might be underestimated by a standard multi-

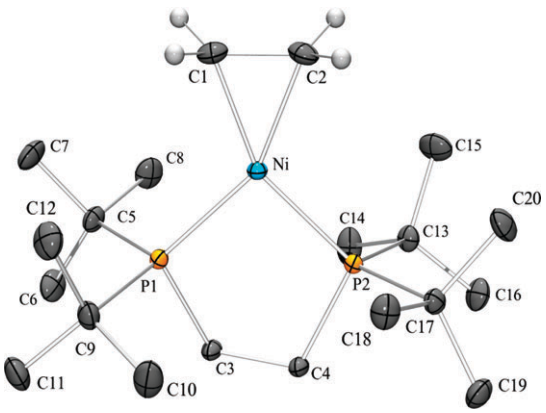


**Fig. 2** Molecular structure of [Ni($\eta^2$-$CH_2CH_2$)dbpe] **1** as obtained from high resolution X-ray diffraction data recorded at $T$ = 110 K; 50% probability ellipsoids. Salient bond distances ($r$) in Å and angles in degrees. Calculated values (ref. 10) in square brackets: Ni–C1 1.9708(4)/[1.962], Ni–C2 1.9715(4)/[1.962], C1–C2 1.4189(6)/[1.422], ∠C1NiC2 42.19(2)/[42.5], ∠P1NiP2 93.456(5)/[93.3].

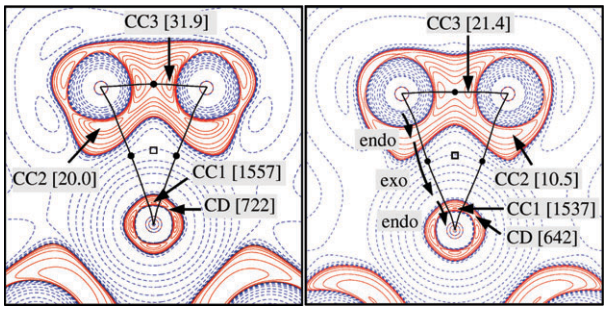


**Fig. 3** $L(\boldsymbol{r})$ contour maps of the experimental (left) and theoretical (right) electron density of **1** in the NiC1C2 plane. Contour levels are drawn at 0.001, $\pm2.0 \times 10^n$, $\pm4.0 \times 10^n$, $\pm8.0 \times 10^n$ $e$Å$^{-5}$, where $n$ = 0, 3, ±2, ±1; extra levels at 11.5, 15.0, 1200 and 1500 $e$Å$^{-5}$; positive and negative values are marked by solid and dashed lines, respectively. BCPs and RCPs are marked by closed circles and squares, respectively; the bond paths are shown by solid lines.The position of salient CCs (1–3) in the valence shell of the C and Ni atoms are marked by arrows.

polar model, which is typically based on single-ξ Slater-type radial functions with energy-optimised exponents (see ref. 9). Otherwise, the endocyclic character at the extremeties of the Ni–C bond paths is a common feature in both theory and experiment; according to Macchi, it is indicative of charge transfer through σ donation.[6] Fig. 1a shows the iso-density contours of the orbital which is mainly responsible for this interaction (HOMO-5) in **1a**, and Fig. 1b depicts its corresponding $L(\boldsymbol{r})$ contour map. However, analysis of the density contours of HOMO-5 reveals that the density contribution from the $p_z$-type AOs at both carbon atoms rather support exo- than endocyclic C–Ni bond path behaviour in the valence space region of the olefinic carbon atoms. Solely, in the valence region of the nickel atom density is accumulated inside the $NiC_2$ ring, and is hence the origin of the inwardly curved bond path in the proximity of the metal.

Since the bond path profile appears to depend on many simultaneous interactions, we have in the following focused our analysis on the valence space of the nickel and olefin carbon atoms, in a search for more reliable charge-density-based criteria with which to analyse the individual contributions of σ and π donation. Population analysis of HOMO-4 reveals that the dominant olefin ← Ni π back-donation in **1a** (and also in **1**) is nearly exclusively spanned by AOs of $p_z$ character at the carbon side and the $d_{yz}$ orbital at the metal side. Hence, the metal to ligand charge transfer represented by this molecular orbital causes local charge depletions (CDs) in the Ni valence shell in regions between the axes of the $yz$ plane (Fig. 1e). Deletion of the charge density contribution of HOMO-4 from the total density hence exaggerates this polarization effect since the residual $d_{yz}$ density at the metal is even further reduced by this manipulation (Fig. 1f).

As a result the global metal polarisation pattern—four regions of charge concentration (CCs) as revealed in the total charge density at the metal centre (Fig. 1e)—appears to be more pronounced in Fig. 1f than in Fig. 1e. Hence, a clear relationship emerges between the polarisation pattern at the transition metal atom and the charge transfer between the metal d-orbitals and the bonding and antibonding π orbitals of

 

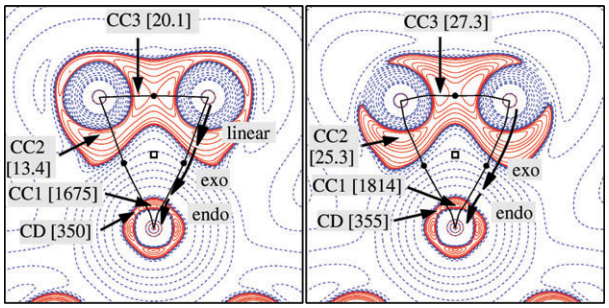


**Fig. 4** $L(r)$ contour maps of **2** and **3** in the $NiC_2$ plane based on the total charge density. Default contour levels as defined in Fig. 3.

the ligand: charge flow from the $d_{yz}$ orbital at the metal (Fig. 1c) to the π* orbital of the olefin clearly distorts the otherwise spherical density distribution of the valence shell of the nickel atom. Hence, significant π donation is accompanied by the evolution of pronounced CCs in the valence shell of the metal atom.[12]

In the same way, we might quantify the influence of σ donation from the ligand to an unoccupied d-orbital at the metal. In the case of our model system **1a**, this interaction is mainly represented by HOMO-5, with a d-orbital of approximate $d_{z^2}$-type symmetry involved in the charge transfer process (Fig. 1a). The contribution of this MO should therefore enhance the polarisation of the metal atom and increase the charge concentration denoted CC1 (1512 $e$Å$^{-5}$) relative to the opposing CC4 (1362 $e$Å$^{-5}$) as revealed by the $L(r)$ map (Fig. 1e).[13]

In order to test our new charge-density-based concept, we have also analysed computationally the bonding in the complexes [Ni(η$^2$-$C_2H_4$)TMEDA] (TMEDA = $Me_2NCH_2CH_2NMe_2$) **2** and [Ni(η$^2$-$C_2F_4$)TMEDA] **3**.[14] **2** and **3** represent models displaying more Lewis-basic Ni centres than **1**, and π back-donation will hence be more pronounced. Furthermore, in **3** the $C_2H_4$ ligand has been replaced by the stronger Lewis acid $C_2F_4$. Accordingly, the extreme DCD case, which favours the description of the $MC_2$ moiety as a metallacyclopropane might appear more appropriate for **3**.

Fig. 4 shows the $L(r)$ contours in the $NiC_2$ plane of **2** and **3**, along with the bond paths. The Ni–C BCPs and hence the corresponding bond paths for **2** and **3** are more separated (0.80 and 0.83 Å, respectively) than they are for **1** (0.60/[0.73] Å), supporting the classification of **2** and **3** as complexes with pronounced metallacyclopropane character. Accordingly, we find more pronounced zones of local charge depletions (CDs) for **2** and **3** (CD ~ 350 $e$Å$^{-5}$) than we do for **1** (CD = 722/[642] $e$Å$^{-5}$), and hence the stronger olefin ← Ni($d_{yz}$) back-donation in **2** and **3** is directly revealed by the topology of the Laplacian.

The major differences in the electronic structures of **1**, **2** and **3** are, however, revealed in the topologies of the charge density in the valence region of the olefin carbon atoms. Here the bond paths display either endocyclic (**1**), linear (**2**) or exocyclic (**3**) profiles (Figs. 3b and 4). Apparently the bond path strongly depends on the location and magnitude of the charge concentrations denoted CC2 and CC3 in the valence shell of the olefin carbon atoms, which appear to direct the NiC bond paths towards their respective locations. Accordingly, the presence of a convex bond path in the valence region of the carbon atom in **3** indicates that CC2 has evolved into a pronounced (Ni–C) bonding CC, implying a significantly sp$^3$ hybridised carbon atom: the bond path is displaced towards CC2 and no longer directed towards CC3 which is the bonding charge concentration of the C=C double bond. The magnitude of CC2 increases from **1** (10.5 $e$Å$^{-5}$) through **2** (13.4 $e$Å$^{-5}$) to **3** (25.3 $e$Å$^{-5}$), in accord with increasing olefin ← Ni($d_{yz}$) back-donation in the same order.

In conclusion, we report a new and improved approach to characterising the synergic bonding in transition metal olefin complexes through charge density analysis. CC2 represents a direct measure of the sp$^3$ character of the olefin carbon atoms, while the metal polarisation pattern allows for a more sensitive measure of the dominant π back-donation component of the bonding than does simple analysis of the bond paths of the $MC_2$ moiety.

## Acknowledgements

This work was supported by the SPP1178 of the Deutsche Forschungsgemeinschaft (DFG).

## References

1 (*a*) J. S. Dewar, *Bull. Soc. Chim. Fr.*, 1951, **18**, C71; (*b*) J. Chatt and L. A. Duncanson, *J. Chem. Soc.*, 1953, 2939.
2 See, for example, G. J. Kubas, *Metal Dihydrogen and σ-Bond Complexes*, Kluwer Academic, Dordrecht, 2001.
3 See, for example,(*a*) K. Kitaura, S. Sakaki and K. Morokuma, *Inorg. Chem.*, 1981, **20**, 2292; (*b*) T. Ziegler, *Inorg. Chem.*, 1985, **24**, 1547; (*c*) J. Li, G. Schreckenbach and T. Ziegler, *Inorg. Chem.*, 1995, **34**, 3245.
4 J. Uddin, S. Dapprich and G. Frenking, *Organometallics*, 1999, **18**, 457.
5 (*a*) R. F. W. Bader, *Atoms in Molecules: A Quantum Theory*, Clarendon Press, Oxford, 1994; (*b*) C. Gatti, *Z. Kristallogr.*, 2005, **220**, 399; (*c*) P. Coppens, *Angew. Chem., Int. Ed.*, 2005, **44**, 6810.
6 P. Macchi, D. M. Proserpio and A. Sironi, *J. Am. Chem. Soc.*, 1998, **120**, 1447–1455.
7 Crystal data for [Ni($CH_2CH_2$)dbpe] **1**: $M_r$ = 405.2, golden prisms; monoclinic, space group $P2_1/n$, $a$ = 8.1610(1), $b$ = 19.7390(1), $c$ = 14.5160(1) Å, $\beta$ = 104.8640(4)°, $V$ = 2260.13(2) Å$^3$; $T$ = 110(1) K; $Z$ = 4, $F$(000) = 888, $D_{calc}$ = 1.191 g cm$^{-3}$, $\mu$ = 0.99 mm$^{-1}$. 262409 Bragg reflections were collected on a Nonius kappa-CCD system with a rotating anode generator (Nonius FR 591; Mo-Kα, $\lambda$ = 0.71073 Å); 31967 independent reflections; $R_{int}$ = 0.037. The data set was corrected for beam inhomogeneity and absorption effects [$T_{min}/T_{max}$ = 0.605/0.654]: 99.7% completeness in the data range sin $\Theta_{max}/\lambda$ = 1.19 Å$^{-1}$. The deformation density was described by a multipole model (ref. 8*a*) in terms of spherical harmonics multiplied by Slater-type radial functions with energy-optimised exponents (see ref. 9 and ESI†). During refinement using the XD program (ref. 8*b*) the H atom positions [$r$($C_{sp^2}$–H) = 1.094, and $r$($C_{sp^3}$–H) = 1.10 Å] and their isotropic thermal parameters (derived from IAM refinements) were fixed. The refinement of 317 parameters against 15032 observed reflections [$F > 2\sigma(F)$, sin $\Theta/\lambda < 1.00$ Å] converged to $R_1$ = 0.0174, $wR$ = 0.0205, GOF = 0.739, and a featureless residual density map. CCDC reference number 276956. For crystallographic data in CIF or other electronic format see DOI: 10.1039/b515171f.
8 (*a*) N. K. Hansen and P. Coppens, *Acta Crystallogr., Sect. A: Cryst. Phys., Diffr., Theor. Gen. Cryst.*, 1978, **A34**, 909; (*b*) T. Koritsánszky, S. Howard, T. Richter, Z. W. Su, P. R. Mallinson and N. K. Hansen, FU Berlin, Germany, 1997.
9 (*a*) E. Clementi and C. Roetti, *At. Data Nucl. Data Tables*, 1974, **14**, 177; (*b*) Z. Su and P. Coppens, *Acta Crystallogr., Sect. A: Fundam. Crystallogr.*, 1998, **A54**, 646; (*c*) P. Macchi and P.

Coppens, *Acta Crystallogr., Sect. A: Fundam. Crystallogr.*, 2001, **A57**, 656.

10 Molecular geometries were fully optimised imposing $C_2$ (**1**, **2**, **3**) and $C_{2v}$ (**1a**) symmetry restraints at the B3LYP/6-311G(d) level of theory using Gaussian 03 (rev. B.03).[15] The topology of $\rho(\boldsymbol{r})_{calc}$ was analysed using a local version of the AIMPAC software package. (*a*) F. W. Biegler-König, R. F. W. Bader and T. Tang, *J. Comput. Chem.*, 1982, **3**, 317; (*b*) J. R. Cheeseman, T. A. Keith and R. F. W. Bader, *AIMPAC program package*, McMaster University, Hamilton, ON, 1994.

11 See for example:W. Scherer and G. S. McGrady, *Angew. Chem., Int. Ed.*, 2004, **43**, 1178.

12 Such metal polarisation was not revealed in the original study by Macchi *et al.*[6] Later refinements, however, also showed a similar polarisation pattern as in our study (P. Macchi, personal communication).

13 This is a secondary polarisation effect, which is difficult to relate to the MO picture since several orbitals are involved in σ donation. The magnitude of CC1 is also correlated with the strength of the π back-donation, and is therefore not a good measure of the σ component.

14 The adduct **2** · ($H_2C$═O) and **3**, have been characterised by earlier X-ray studies; (*a*) W. Schröder, K. R. Pörschke, Y.H. Tsay and C. Krüger, *Angew. Chem., Int. Ed. Engl.*, 1987, **26**, 919; (*b*) W. Kaschube, W. Schröder, K. R. Pörschke, K. Angermund and C. Krüger, *J. Organomet. Chem.*, 1990, **389**, 399.

15 M. J. Frisch, *et al.*, *GAUSSIAN 03 (Revision B.3)*, Gaussian, Inc., Pittsburgh, PA, 2001.



 